Light-activated superhydrophobicity of the Sustainable Micro-structured Spent Coffee Grounds-Based Interface via Fatty acids Modulation

Seyed Shahrooz Zargarian[a*], Salvio Suárez-García[b], Javier Saiz-Poseu[b], Daniel Ruiz-Molina[b], and Filippo Pierini[a*]

Seyed Shahrooz Zargarian (shzargar@ippt.pan.pl), Filippo Pierini (fpierini@ippt.pan.pl)

[a]Department of Biosystems and Soft Matter, Institute of Fundamental Technological Research, Polish Academy of Sciences, Pawińskiego 5B, Warsaw 02-106, Poland

Salvio Suárez-García (salvio.suarez@icn2.cat), Javier Saiz-Poseu (javier.saiz@icn2.cat), Daniel Ruiz-Molina (dani.ruiz@icn2.cat)

[b]Catalan Institute of Nanoscience and Nanotechnology (ICN2), CSIC and BIST, Campus UAB, Bellaterra, 08193 Barcelona, Spain

[*]Corresponding authors:

Seyed Shahrooz Zargarian (shzargar@ippt.pan.pl)

Filippo Pierini (fpierini@ippt.pan.pl)

Correspondence to: Filippo Pierini (fpierini@ippt.pan.pl)

Abstract

The global consumption of coffee results in the disposal of vast amounts of spent coffee grounds (SCG), posing significant environmental challenges. Herein, we address this issue by developing an innovative, eco-friendly method to achieve superhydrophobicity using SCG. By repurposing this abundant biowaste, we developed a sustainable approach that avoids the use of harsh chemicals and energy-intensive processes typically associated with conventional methods. Our procedure involves wet ball milling of SCG in ethanol to produce microparticles, followed by electrospraying to create a micro-structured interface. A mild annealing treatment at 90°C successfully transformed the SCG interface from hydrophilic to superhydrophobic, reaching a contact angle of approximately 151° and a rolling-off angle of 8°. The resultant interface exhibited remarkable water repellency and self-cleaning properties, effectively repelling various liquids. XPS analysis revealed that the migration of fatty acids to the surface during annealing played a crucial role in lowering surface energy, thereby driving the hydrophilic-to-superhydrophobic transition. Furthermore, we demonstrated that solar-induced heating can effectively activate the same superhydrophobic properties, providing a practical and energy-efficient alternative to traditional thermal treatments. This method illustrates the role of light-activated fatty acid modulation in achieving superhydrophobicity and highlights the potential of SCG biowaste as a valuable resource for sustainable material applications.

1 Introduction

Superhydrophobic and superoleophilic materials exhibit extraordinary surface properties, showing high water repellency (contact angle >150°), low water droplet roll-off angles (<10°), and a strong affinity for oil (contact angle <5°).[1–3] These remarkable properties result from a combination of low surface energy and high surface roughness. To achieve both superhydrophobic and superoleophilic conditions, the surface energy of the final layer must fall within the range of 30 mN/m < γ < 72 mN/m.[4] While chemical modification can influence the surface energy, it alone is limited to achieving superhydrophobicity.[5] The key to extreme water repellency lies in manipulating surface roughness to generate a microstructure that traps air pockets beneath the water droplet.[6,7] This air cushion effectively reduces the contact area between water and the surface, further enhancing water repellency. A hierarchical structure, where nanoscale roughness is superimposed on top of larger microstructure features, is particularly effective in achieving superhydrophobicity, as exemplified by the lotus leaf, a natural example of this phenomenon.[8,9] These unique characteristics have opened up a plethora of applications, particularly in environmental remediation and oil-water separation.[4,10] Superhydrophobic surfaces are widely used in self-cleaning coatings,[11,12] while the superoleophilic property facilitates the collection and recovery of oil spills and the efficient separation of oil-water mixtures.

Traditional methods for creating superhydrophobic and superoleophilic surfaces typically involve chemical modifications[13] or treatments such as pyrolysis[14] or calcination[15]. However, these conventional approaches are associated with energy-intensive processes, often requiring high temperatures and the use of harsh chemicals, which raises concerns about toxicity and environmental sustainability. For instance, a recent study on fabricating superhydrophobic

cellulose-based membranes involved immersing filter paper in acetonitrile solutions of toluene diisocyanate and N-(2,4-di aminophenyl) maleimide for three cycles, a process that involves the use of harsh solvents.[13] Another study by Duan *et al.* reported the fabrication of superhydrophobic and superoleophilic coatings using ball-milled biochar loaded on a melamine foam skeleton, which required a pyrolysis step at 700 °C, consuming significant energy.[14] Similarly, Guo *et al.* described the preparation of a superhydrophobic construct using silica nanoparticles, prepared via a sol-gel method and coated on stainless steel mesh.[15] This process involved multiple steps, including dipping the metallic mesh into SiO_2 sol, drying in an oven, and a calcination step at 300 °C, further emphasizing the energy-intensive nature of these traditional methods.

Transitioning from traditional methods that often involve environmentally detrimental practices, there is a growing emphasis on adopting more eco-friendly materials and processes for producing superhydrophobic interfaces and membranes. Embracing this eco-friendly paradigm involves careful selection of materials and fabrication practices. According to Bayer,[9] eco-friendly practices should encompass the entire fabrication process and avoid excessive heat. Additionally, since many coatings are formulated in suspensions, it is crucial to advocate for the use of green solvents, which should be biomass or plant-based rather than petroleum-derived. For instance, deep eutectic solvents,[16] triethyl phosphate,[17] and ethanol[18] have been employed as green solvents in the fabrication of superhydrophobic melamine sponges, PVDF membranes, and polyamide fibrous membranes, respectively. Conversely, in terms of materials, the shift towards eco-friendly alternatives prioritizes inherently earth-friendly substances, such as natural, biodegradable, and nontoxic materials or those derived from organic waste.[19] Utilizing these materials addresses the need for sustainable resources and contributes to reducing pollutants released into the environment. For instance, a superhydrophobic cellulose-based aerogel was fabricated through a one-step process involving the deposition of copper nanoparticles on cellulose fibers extracted from renewable natural sisal in a liquid phase.[20] Additionally, an eco-friendly strategy involving starch nanoparticles and polydimethylsiloxane composites was employed to produce superhydrophobic coatings with hierarchical micro and nanostructures.[21] In a recent study, bamboo powder was pivotal in enhancing PVDF foam, producing a highly porous and superhydrophobic membrane via an organic solvent-free process.[22] Despite the commendable sustainable approach of using bioderived and organic waste-derived materials in these studies, these substances still required chemical treatment or conversion into biochar to achieve superhydrophobicity due to their inherent hydrophilic nature.

In this scenario, spent coffee grounds (SCG) represent a promising biowaste source with significant potential for sustainable material innovation. With an estimated daily consumption of 2.25 billion cups of coffee worldwide,[23] approximately 18 million tons of wet SCG are generated yearly,[24] posing a growing environmental concern due to its potential impact on landfilling, soil degradation, and water pollution.[25,26] However, the abundance and ease of acquisition solidify its position as a promising feedstock for sustainable materials. Moreover, the composition of SCG makes it a valuable feedstock for sustainable materials. The composition of SCG varies on the type of coffee beans used and brewing method, though, in general, it contains approximately 8.6-13% cellulose, 32-42% hemicellulose, 20-30% lignin, 35-38% sugar monomers (mannose, galactose, and arabinose), 2-19% fatty acids, and 1-3% minerals.[27–31] Given lignocellulose composition,[32] SCG is inherently hydrophilic, exhibiting a strong affinity for water. Despite this, research has explored its potential for designing superhydrophobic platforms. Few studies have explored

various strategies to utilize SCG in fabricating such materials. For instance, in a study focusing on dye removal from effluents, SCG was utilized to produce activated carbon through chemical activation with NaOH and subsequent carbonization at 300 °C.[33] Another study extracted lignin and other organic substances from SCG.[34] The resulting delignified SCG was then reacted with an organosilicon compound in n-heptane, forming a superhydrophobic material. These studies suggest that the inherent hydrophilic nature of SCG necessitates chemical treatment or conversion into biochar to achieve superhydrophobicity.

While the intrinsic chemical composition of SCG presents challenges for achieving the low surface energy required for superhydrophobicity, the geometrical architecture of the surface is an equally critical factor. As mentioned, superhydrophobicity is influenced by both the chemical composition and the hierarchical micro-nano structured morphology of the surface.[35,36] In this context, electrospraying emerges as a robust and scalable technique for fabricating micro-structured surfaces with precise control over surface morphology.[37,38] It has gained significant traction in fabricating superhydrophobic interfaces due to its ability to produce thin, uniform layers with controlled microstructures. Numerous studies have demonstrated the effectiveness of electrospraying in producing superhydrophobic interfaces with exceptional water-repellency and self-cleaning properties. For instance, a highly transparent self-cleaning superhydrophobic surface was prepared by electrospraying an organosilane-coated alumina precursor.[39] By simply controlling the spraying time, a coating with excellent superhydrophobicity and transparency in the visible range was achieved. Another team studied the deposition of morphology-controlled polyimide particles through electrospraying, enabling them to fabricate highly hydrophobic multilayered films with tunable morphologies.[40] Moreover, electrospray deposition has been employed to prepare corrosion-protective coatings for metal substrates.[41] The electrosprayed carbon layers exhibit remarkable adherence and highly porous structures, leading to Cassie–Baxter type superhydrophobicity, effectively hindering corrosion.

Herein, we report an eco-friendly method to achieve superhydrophobicity using SCG without resorting to harsh chemicals or energy-intensive processes. Our innovative approach involves wet ball milling SCG to produce a suspension of microparticles in ethanol, followed by electrospraying to produce a micro-structured interface. A mild annealing treatment at 90°C effectively transforms the SCG interface from hydrophilic to superhydrophobic and superoleophilic. This method stands out due to its simplicity, the use of a green solvent, and its minimal environmental impact, offering a sustainable alternative to traditional techniques. We extensively analyze the chemical structure and morphology of the SCG-based interface, elucidating the mechanism behind the hydrophilic-to-superhydrophobic transition. Additionally, we demonstrate the interface's effectiveness in self-cleaning applications. This work represents a pioneering step in showcasing the feasibility of achieving special wettability from a readily available biowaste resource with minimal intervention, opening up new avenues for sustainable and environmentally friendly applications of SCG.

2 Experimental

2.1 Materials

Ethanol was used as received without additional drying or degassing (Sigma-Aldrich). All other reagents were obtained from Sigma-Aldrich or Merck unless otherwise specified.

2.2 Sample preparation

2.2.1 SCG preparation

SCG was sourced from a Costa Coffee outlet in Warsaw, Poland. The organic waste was then subjected to a sequential procedure illustrated in Fig. 1a, starting with an initial purification step by washing the grounds with deionized water (DW) (Milli-Q water filtering system, Millipore, Bedford, MA) to eliminate any water-soluble impurities. The cleaned SCG was then dried and sieved to achieve a uniform particle size distribution with diameters below 300 μm. Further size reduction was accomplished using dry and wet ball milling techniques described elsewhere.[42] In the wet ball milling process, ethanol, an eco-friendly solvent, or DW, was added to the SCG powder to facilitate particle dispersion, achieving a concentration of 12% w/v. These suspensions were transferred into tungsten carbide milling chambers. The milling operations were conducted using a high-energy planetary ball mill (Fritsch Pulverisette 5). The process resulted in a fine microparticle suspension of SCG in either ethanol (Wet ethanol ball milled, abbreviated to **WEBM**) or DW (Wet water ball milled, abbreviated to **WWBM**), which was subsequently sealed and stored at room temperature for future fabrication steps. The same milling procedure was applied to the SCG powder (Dry ball milled, abbreviated to **DBM**) for the dry ball milling process.

2.2.2 Fabrication of the interfaces

The electrospraying method was employed to fabricate a micro-structured interface using SCG microparticles. The WEBM (the SCG suspension in ethanol) was placed in a 1 mL syringe fitted with a 20-gauge needle and subjected to a high voltage of 12 kV, with the flow rate set at 450 μL/h. The experiments were carried out at room temperature and a relative humidity of 20%. During the process, the electrospraying of the WEBM suspension produced a fine spray of particles. A rotary drum spinning at 600 RPM was used to collect the SCG microparticles. After approximately two hours, a brownish interface, referred to as RSCG, was formed, with an approximate thickness of 60 μm. Simultaneously, the WEBM suspension was drop-casted onto a metallic surface (RSCG cast). Subsequently, all products underwent a uniform mild annealing treatment (at 90°C for 6 hours), categorizing the samples with an "H" designation, representing HSCG electrosprayed and cast. These samples will be referred to as HSCG or RSCG unless otherwise specified.

2.3 Spectroscopic, morphological and thermal characterization

To measure the particle size and distribution of WEBM, WWBM, and DBM, a Malvern Mastersizer 3000 particle size analyzer equipped with a HydroMV2000 attachment was utilized. Approximately 300-500 mg of samples were used for each test. The average particle size distribution of the SCG was determined using this device. Fourier transform infrared (FTIR) analyses were performed in attenuated total reflectance (ATR) mode using a Bruker Vertex70 FTIR spectrometer, recording the wavenumber range from 4000 to 400 cm^{-1} with a resolution of 2 cm^{-1} after 12 scans per sample.

The variable-temperature FTIR spectra were recorded with a Hyperion 2000 microspectrometer coupled to a Vertex 80 spectrometer (both from Bruker Optik GmbH, Germany). The analyzed

range was 4000-600 cm^{-1}, with a resolution of 4 cm^{-1} and 24 scans. The samples were placed on a copper holder and then directly heated on a homemade heating stage consisting of a 19 W metal ceramic heater (Thorlabs Inc., New Jersey, USA) controlled by a Rex-C100 digital temperature controller (Iriisy, China). After reaching the corresponding set point (23 ºC, 60 ºC, 80 ºC, and 130 ºC), a delay time of 5 min was used before the measurement to let the sample thermally stabilize. All the data was treated with OPUS version 7.5 (Bruker) software.

UV-Vis-NIR analyses were conducted in the solid state using diffuse reflectance mode with a Perkin Elmer Lambda 1050+ (Madison, WI, USA) provided by Pro-Environment Polska Sp. z o.o. (Warsaw, Poland). Measurements were taken over a wavelength range of 250 to 1000 nm, with a scanning rate of 1 nm per minute.

Contact angle measurements were performed using an OCA 15EC goniometer. Droplets of 5 µL were placed on the surface of the SCG's interface, and the contact angles of three drops were measured and averaged using ImageJ.

The static contact angle and the roll-off angle experiments were performed with a DSA25S instrument (Krüss GmbH, Hamburg, Germany). The drops were dispensed on the samples with a 100 µl syringe through a 0.520 µl diameter needle and an automatic software-controlled dosing system. The analysis of the drops and the control of the tilting during the roll-off experiments were carried out with the KRÜSS ADVANCE software, which used the sessile drop technique and the Ellipse tangent method in both cases to obtain the contact angle values. The volume used for the experiments was 5 µl in the contact angle and the roll-off angle measurements. The tilting was recorded from 0° to 90°, with a rate of 1 °/sec.

Varaible-temperature micrographs were obtained using a scanning electron microscope (SEM, FEI Quanta 650 FEG, Thermo Fisher Scientific, Eindhoven, The Netherlands) in secondary electron mode and operating at 20 kV. All samples were fixed on an SEM heater holder and directly heated at different temperatures (26 ºC, 46 ºC, 66 ºC, 86 ºC, 116 ºC, and 200 ºC). After reaching the corresponding set point, a delay time of 5 min was used before the measurement to let the sample thermally stabilize.

Samples were also imaged using a scanning electron microscope (SEM) (JSM-6010PLUS/LV, In TouchScope microscope). Depending on the sample, images were captured at varying accelerating voltages (7 to 12 kV) and magnifications. X-ray diffraction (XRD) measurements were performed on all samples using a Bruker D8 Discover diffractometer in Bragg-Brentano geometry. The analysis covered an angular range of 5-60° (2θ), with data collected at each point using a step size of 0.02 per 1.0 s. Thermogravimetric analysis (TGA) was carried out on the samples (minimum 50 mg per sample) using a Perkin-Elmer TGA 8000 analyzer (Shelton, USA), also supplied by Pro-Environment Polska Sp. z o.o. (Warsaw, Poland). The measurements were conducted from 35°C to 800°C in a nitrogen atmosphere (N_2 supplied by Air Liquide Sp. z o.o., Cracow, Poland) at a heating rate of 3 °C per minute, with a balance purge flow rate of 40 mL per minute. For TGA and XRD measurement, the WEBM suspension was dispensed in a Petri dish, dried at room temperature to yield RSCG Powder, and annealed as previously mentioned to obtain HSCG Powder.

2.4 X-Ray Photoelectron Spectroscopy (XPS)

XPS measurements were performed with a Phoibos 150 analyzer (SPECS EAS10P GmbH, Berlin, Germany) in ultra-high vacuum conditions (based pressure 10^{-10} mbar, residual pressure around 10^{-7} mbar). Monochromatic Al Kα line was used as an X-ray source (1486.6 eV and 300 W). The electron energy analyzer was operated with a pass energy of 50 eV. The hemispherical analyzer was located perpendicular to the sample surface. The data was collected every eV with a dwell time of 0.5 s. A flood gun of electrons, with energy lower than 20 eV, was used to compensate for the charge. The reference was set for C-C at 284.8 eV. All the data was treated with CasaXPS version 2.3.17PR1.1 (Casa Software LTD, Teignmouth, UK) and OriginPro version 8.0988 (OriginLab Corporation, Northampton, MA, USA) software.

2.5 Assessment of the photothermal properties

The photothermal properties of RSCG were assessed under conditions simulating one sun irradiation. A solar simulator from Abet Technologies, model 10500, was used. The device is equipped with a 150 W Xe Arc Lamp as the light source. The optical system of this device produces a focused 25 mm beam, with one sun output achievable over an illuminated field up to 35 mm in diameter. To capture and analyze the spatial heating distribution and temperature profile generated by the solar simulator, a high-resolution infrared camera (FLIR, A655sc) was utilized. The camera was paired with specialized software (FLIR ResearchIR Max), enabling the recording and subsequent processing of the thermal data collected during the experiments.

3 Discussion

First, the particle size distribution of SCG obtained through various ball-milling methods was studied (Fig. 1b). Both dry ball milling and wet ball milling in water yielded particles with a broad size distribution, ranging from 3 to 65 µm. Although the particle size and distribution of dry ball-milled SCG were not significantly different from those of water ball-milled SCG, it should be noted that forming a suspension from the former is very challenging due to extensive agglomeration. This agglomeration hinders the formation of a homogeneous suspension. Conversely, wet ball milling in ethanol significantly reduced the average particle size to 8 µm, resulting in a much narrower size distribution. Despite the high concentration of SCG in ethanol (12% w/v), the small size and good uniformity of WEBM microparticles achieved through wet ball milling in ethanol resulted in a fairly stable suspension, making it suitable for spraying. Therefore, the results suggest that the choice of solvent in the ball-milling process plays a critical role in controlling the particle size and distribution.

To investigate the influence of different ball-milling methods on the chemical composition of SCG, FTIR spectroscopy was employed to analyze the sample spectra within the range of 500 to 4000 cm^{-1}. Fig. 1c illustrates the FTIR absorbance spectral peaks, recording diverse strong, broad, and weak intensities of absorption corresponding to the majority of functional groups present in SCG. The broadband occurring between 3000 and 3700 cm^{-1}, with a maximum at 3372 cm^{-1}, corresponds to the O–H and N–H stretching vibration, suggesting the presence of free hydroxyl groups and bonded O–H bands of carboxylic acids.[43] This region is primarily attributed to alcohol,

phenols, or carboxyl functional groups and features intra- and intermolecular hydrogen bonding, characterizing the distinctive peaks associated with crystalline cellulose in SCG.[44] The sharp peaks observed at 2920 and 2830 cm^{-1} can be attributed to C-H stretching vibrations in aliphatic compounds, indicating the presence of organic moieties.[45] Peaks at 1750 and 1640 cm^{-1} are associated with the stretching vibrations of carbonyl (C=O) and C=C bonds, respectively, suggesting the presence of aromatic and carbonyl-containing compounds.[46] The weak peak at 1355 cm^{-1} may indicate other functional groups or vibrational modes present in the sample. The FTIR spectra of the three samples exhibited similar patternsThe FTIR spectra revealed no new peaks or the disappearance of existing peaks, indicating that the ball-milling conditions neither introduced nor removed any major chemical constituents from the as-obtained SCG.. Furthermore, the relative intensities of the characteristic peaks in the FTIR spectra appeared to be consistent across all three samples. This observation suggests that ball milling might not have significantly affected the fundamental chemical composition of SCG. To further investigate the influence of different ball-milling methods on the chemical composition, diluted suspensions (0.3% w/v) of WWBM and WEBM SCG were prepared, and their UV-Vis spectra were compared. The UV-Vis spectra of the two samples (Fig. 1d) demonstrated remarkable similarity. However, despite having similar concentrations, the WEBM sample exhibited higher intensity compared to WWBM. This elevated intensity is likely attributable to the smaller particle size of WEBM, which promotes a more uniform dispersion in the solution, allowing for higher absorption of UV-Vis radiation and, consequently, higher absorbance values. This observation further reinforces the notion that ball milling primarily affects particle size rather than the chemical composition of SCG.

From a morphological point of view, SEM images of DBM, WWBM, and WEBM revealed a rough, heterogeneous surface with a variety of features, including irregular-shaped particles of different sizes (Fig. 1e). These features arise from the complex composition of SCG, which comprises cellulose, hemicellulose, lignin, and other organic compounds, along with mineral constituents. No porous structure was observed, indicating that ball milling primarily affected particle size rather than overall surface morphology. Interestingly, all samples displayed a scattered pasty substance on the surface of the SCG particles, suggesting the displacement or rearrangement of specific components, possibly originating from the internal layers of the as-obtained SCG. However, the presence of the mentioned pasty substance was less pronounced in the DBM sample and more vivid in WEBM, suggesting that the relocation of those substances happens more efficiently during ethanol ball milling compared to dry ball milling. Moreover, while both water and ethanol act as lubricants during wet ball milling, ethanol acts as a better solvent for the non-lignocellulosic components of SCG and further contributes to particle breakage.

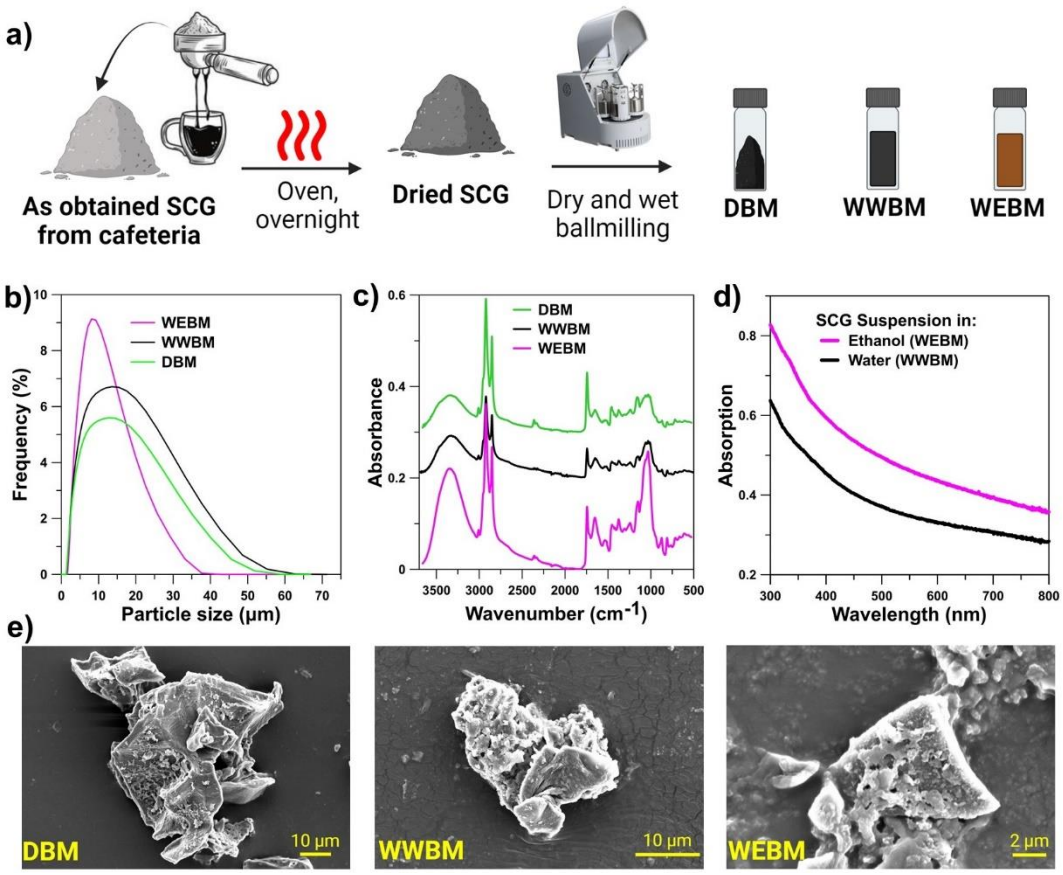

Figure 1: Overview of the spent coffee grounds (SCG) sample preparation and characterization. a) Schematic illustration of the sample preparation process, depicting the collection of SCG from a cafeteria, followed by drying in the oven and ball milling in different conditions: dry ball milling (DBM), water ball milling (WWBM), and ethanol ball milling (WEBM). b) Particle size distribution of SCG samples prepared, revealing the effect of ball-milling conditions on SCG particle size. c) FTIR spectra of DBM, WBM, and WEBM. d) UV-vis spectra of dilute suspensions of WWBM and WEBM. e) SEM images of the samples.

In the next step, electrospraying was used to fabricate fine interfaces of SCG. One of the key factors influencing the success of the electrospraying process is the solvent selection.[37,38,47] Ethanol is an excellent solvent for electrospraying due to its rapid evaporation rate and low surface tension, which are crucial for achieving the desired nano- or microstructures. The low surface tension of ethanol (22.1 mN/m)[48] compared to deionized water (72.6 mN/m)[49] allows for the formation of stable and uniform droplets during electrospraying. This is because lower surface tension reduces surface tension-induced forces that tend to destabilize droplets, making them less likely to coalesce.[50] Moreover, ethanol's higher vapor pressure (~7.0 kPa at 23 °C) compared to water (~2.8 kPa at 23 °C) facilitates faster evaporation and helps the formation of a uniform interface.[51] In our study, the ethanol-based suspension of SCG particles (WEBM) possesses smaller particles with a narrower size distribution compared to DBM and WWBM. Additionally, the presence of ethanol in WEBM further enhances its suitability for electrospraying by facilitating rapid evaporation and promoting the formation of stable microdroplets. As a result of these advantages, WEBM was selected as the optimal suspension of SCG microparticles for subsequent processing steps.

WEBM underwent an electrospraying process at room temperature and relative humidity, as illustrated in Fig. 2a. A fine interface of SCG microparticles on a metallic surface was achieved and dried at room conditions (RSCG). Separately, RSCG was annealed at 90 °C for 6 h (HSCG). Contact angle measurements were conducted by placing 5 µL deionized water droplets onto the surface of the samples (Fig. 2b). As expected, water quickly spread on the RSCG surface, resulting in a contact angle of zero within less than 1 min. However, we observed an intriguing manifestation of a superhydrophobic behavior in SCG, as evidenced by the remarkable contact angle of HSCG, calculated to be 151.6 ± 1.7° at the start of the experiment. Notably, it was challenging to place a water droplet directly on the HSCG surface. As shown in Sup. Fig. 1, the interface surface approached the water droplet, made contact, and then retracted, leaving the droplet hanging by the needle tip. On the other hand, the HSCG interface demonstrated superoleophilic properties, allowing non-polar liquids such as oils to rapidly spread across its surface. As shown in Supplementary Video 1, a drop of olive oil, with a surface tension of approximately 33 mN/m at 20 °C,[52] was placed on the HSCG, which wetted the surface instantly. The superhydrophobicity of the HSCG was further demonstrated by its ability to readily repel water droplets (Fig. 2c and Supplementary Video 2). The ability of water droplets to roll off the HSCG surface has significant implications for its potential applications. Furthermore, as shown in Sup. Fig. 2 and Supplementary Video 3, a single drop of water can be easily guided across the surface using a needle tip. This characteristic is another hallmark of superhydrophobic surfaces and can be attributed to the combination of low surface energy and the formation of a stable air layer that effectively prevents water penetration. Notably, while the HSCG cast (the annealed drop-casted WEBM on a metallic surface) exhibited some degree of hydrophobicity, it was less effective compared to the HSCG electrosprayed (Sup. Fig. 3). Specifically, the HSCG cast allowed water to wet the surface after approximately 20 min, and maneuvering a water droplet across its surface was not feasible. This difference highlights the advantage of the micro-structured interface achieved through electrospraying, which promotes surface roughness and the formation of a more stable air cushion.[53] This air cushion, in turn, enhances the superhydrophobicity by preventing water from making prolonged contact with the surface.

Water repellency is essential for preventing surface contamination and facilitating self-cleaning properties. As shown in Supplementary Video 4, the rolling behavior of water droplets on HSCG further enhances the self-cleaning property, as droplets carrying accumulated dirt are effortlessly removed from the surface. The remarkable water repellency of HSCG extended beyond water itself, encompassing a diverse range of liquids. Droplets of tea, milk, coffee, and liquid dyes like methylene blue, curcumin, and rhodamine, dissolved in water, exhibited exceptional stability when placed on the HSCG surface (Fig. 2d). These droplets maintained their spherical shape without spreading, retaining their integrity until complete evaporation. This phenomenon demonstrates the excellent anti-wetting properties of HSCG. Even a drop of WWBM, the highly concentrated suspension of SCG ball-milled in water, retained its spherical shape on the HSCG-coated surface, demonstrating the interface's ability to repel even its own constituents. The average roll-off angle for water droplets on HSCG was calculated to be 8.5° ± 0.7° (Fig. 2e), indicating that the droplets were able to easily detach from the surface and roll off without any significant resistance.

Next, the morphology of the interface was examined. However, obtaining clear SEM images of the electrosprayed SCG interface proved to be extremely challenging, likely due to the very low conductivity of the particles and the relatively high thickness of the interface, which resulted in significant surface charging (Sup. Fig. 4). To address this challenge, a solution of low molecular

weight polyethylene glycol (PEG) in ethanol (10% w/v, Mw 6000) was electrosprayed on top of the RSCG, which facilitated the acquisition of clearer SEM images (Fig. 2f). The SEM images reveal the successful fabrication of a micro-structured interface from SCG microparticles. At low magnification, the overall micro-structured morphology of the interface is evident. The biowaste microparticles appear as irregularly shaped entities, with an average area of 96 ± 2.1 μm^2 and an average diameter of 9.6 ± 0.4 μm, dispersed evenly throughout the interface's construct. Higher magnification images provide a closer look at the SCG particles, highlighting their irregular shape, standing as pillars.

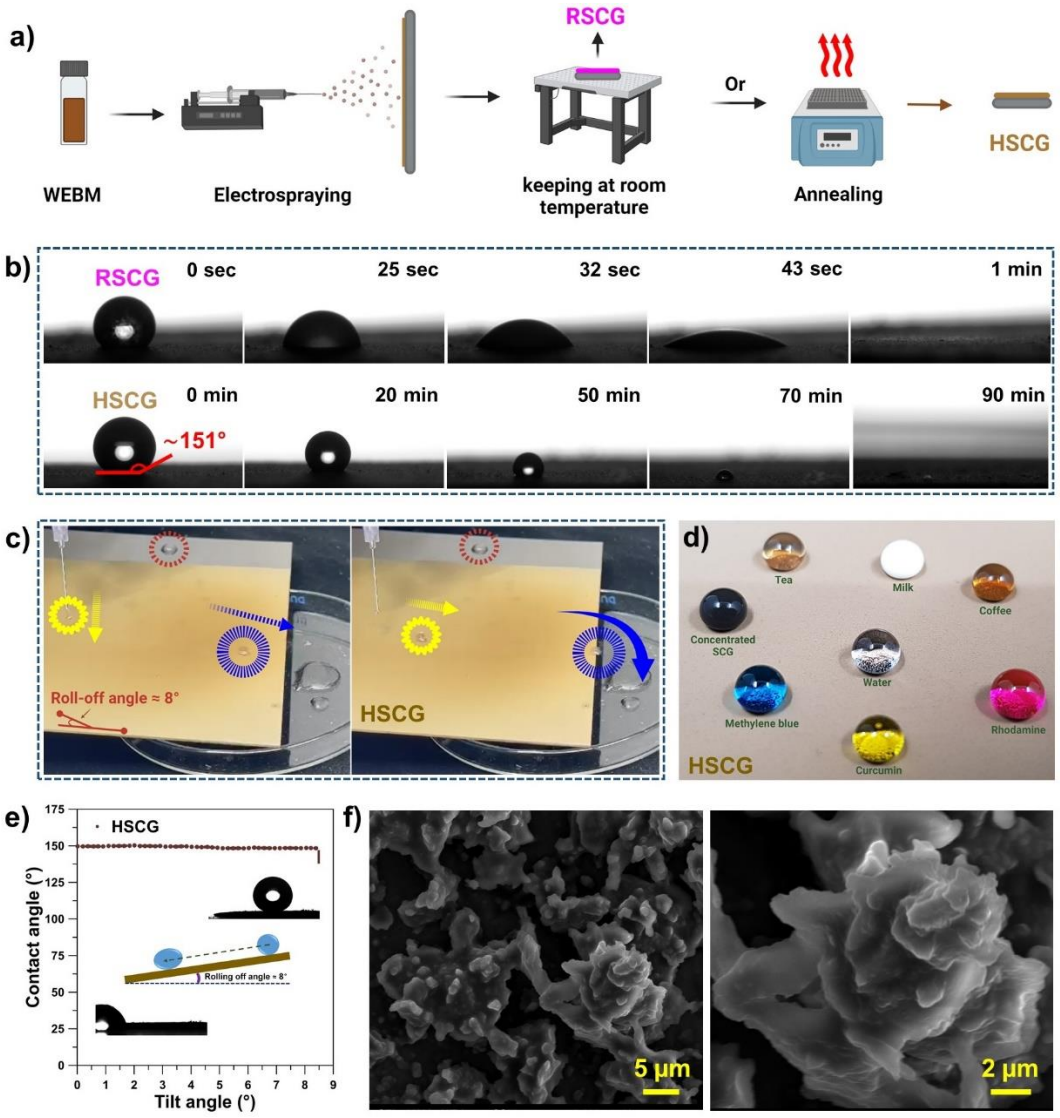

Figure 2: SCG electrospraying and transition to superhydrophobicity. a) Schematic illustration of the electrospraying process of WEBM suspension on a metallic substrate, resulting in an interface. The coated substrate was either dried at room temperature (RSCG) or subjected to an annealing treatment (HSCG). b) Contact angle measurements on RSCG and HSCG demonstrate remarkable HSCG superhydrophobicity. Time scales of decremental contact angle can range from seconds for RSCG to several minutes for HSCG. c) Camera photos show water droplets placed on the tilted HSCG surface, causing them to roll off. A water droplet can be seen placed on the uncoated part of the metallic surface, which remained stationary. d) Repellence of the superhydrophobic HSCG to various liquids. e) Contact angle and tilt threshold for HSCG

superhydrophobic interface. f) SEM images of SCG microparticles at different magnifications, revealing a hierarchical micro-roughness reminiscent of the lotus leaf surface

To determine the chemical and structural evolution of SCG during the annealing process, we first investigated the absorption spectra of RSCG using an FTIR spectrometer equipped with a sample heater plate for *in situ* measurements during a controlled temperature ramp (Fig. 3a). The electrosprayed SCG microparticles at room temperature (RSCG) exhibited all the characteristic features of the SCG chemical composition previously discussed. Then, as the temperature increased, the bimodal sharp peak at 1030 cm^{-1}, likely associated with C-O stretching vibrations[45,54] indicative of ether linkages in cellulose, hemicellulose, and lignin, remained unchanged. However, the intensity of the broad peak between 3100 and 3500 cm^{-1} gradually decreased, corresponding to the hydroxyl group (O–H) stretching vibration,[55] indicating moisture release. This peak gradually shifted to higher wavenumbers as the temperature increased, reflecting diminished hydrogen bonding interactions between the functional groups of SCG. The peak at 1640 cm^{-1}, associated with C=C bond stretching vibrations,[56] also decreased in intensity, suggesting the release of volatile aromatic compounds, such as pyrazines and pyridines, due to the temperature increase. These compounds are significant in SCG[57] and contribute to its characteristic coffee aroma.[58]

In the next step, the XRD pattern of the HSCG and RSCG powders was systematically investigated within the 2θ range of 5–60°. The diffraction peaks for both samples exhibit the characteristic amorphous or poorly crystalline phases associated with SCG (Fig. 3b). In line with established observations, a predominant feature is the presence of a broad peak spanning 2θ values of approximately 10° to 30°, with maxima at 20°, corresponding to the (002) crystal plane,[44,59] aligning with the expected XRD pattern of lignocellulosic materials.[60] Additionally, narrower peaks are discernible at 35.5°, 37°, 43.5°, and 48°. Of particular note is the peak at 43.5°, attributed to the (100) crystal plane, which stands out prominently and exhibits characteristics reminiscent of turbostratic structures, similar to those observed in graphene.[61] While no significant structural alteration is apparent, a subtle decrease in the diffraction peak intensity at 43.5° is observed for HSCG compared to RSCG. It is reported that in the pyrolysis reaction of SCG, an elevation in temperature leads to an increased intensity of the 43.5° peak,[44] linked to the formation of carbon-rich cellulose and the concurrent destruction of lignocelluloses. This contrasts with our observations for HSCG, suggesting that the mild post-heat treatment applied in our study has a negligible effect on the core structural properties of SCG, indicating the material's structural integrity within the examined parameters.

TGA analysis was also conducted on RSCG and HSCG powders to investigate their thermal behavior and the effects of the annealing process (Fig. 3c). Initially, RSCG exhibited an 8.3% weight loss up to 100 °C, compared to only 2.7% for HSCG, indicating the annealing process's impact on moisture content. This significant reduction in weight loss for HSCG suggests that the annealing effectively removes loosely bound water, making the interface superhydrophobic and resistant to moisture reabsorption. The persistence of an approximately 6% weight difference between RSCG and HSCG over the entire temperature range up to 800°C confirms that this initial moisture-induced weight difference remains constant, highlighting the role of annealing in eliminating hygroscopic content without substantially altering the fundamental composition of the SCG particles. Furthermore, the shift in the primary decomposition peak from 295°C in RSCG to

305°C in HSCG, observed in the derivative thermogravimetric analysis (DTGA), suggests a degree of chemical stabilization induced by the annealing process. The mentioned 10 °C increase in the peak decomposition temperature for HSCG implies that the annealing reduces moisture content and contributes to the thermal stabilization of the SCG microparticles. This stabilization may involve removing or transforming volatile compounds[62] that might otherwise decompose at lower temperatures, such as trapped water, aromatic compounds, or small organic molecules. This hypothesis is consistent with the reduced volatile release observed in the FTIR analysis. The reduced volatility and increased thermal resistance of these compounds in HSCG may explain the observed shift in the DTGA peak, suggesting that annealing promotes the formation of more thermally stable structures in the SCG matrix. Additionally, the small shoulder observed in the DTGA curve of RSCG between 350°C and 450°C, which is not present in HSCG, further confirms that annealing leads to the release of some volatiles, causing a 0.6% weight difference between RSCG and HSCG, thus stabilizing the thermal profile of the material.

The superhydrophobicity observed in HSCG can generally be attributed to two key factors: low surface energy and surface roughness.[5,63] Given that no fundamental chemical changes were observed in the FTIR, XRD, and TGA analyses, and considering that morphology plays a critical role in superhydrophobicity, it was essential to assess whether any morphological alterations occurred during the annealing process. SEM imaging of RSCG, conducted with a device equipped with temperature ramping capability, revealed no noticeable changes in the surface morphology during the heating process up to 200 °C (Sup. Fig. 5). Therefore, the superhydrophobic behavior of HSCG is not due to morphological alterations. This leaves changes in surface composition after the mild post-process as the likely cause. To evaluate this hypothesis, it was necessary to investigate the surface composition of SCG microparticles for both RSCG and HSCG. XPS is a powerful tool for analyzing the surface chemistry of materials, offering detailed insights into their elemental composition and molecular structure. Given that the superhydrophobic properties of a coating are closely linked to its surface composition and chemical features, utilizing XPS to assess these characteristics is essential for understanding the underlying mechanisms of water repellency.

The survey XPS spectrum of RSCG shows the characteristic peaks of C 1s and O 1s, the main components of SCG (Fig. 3d). Nitrogen was detected on the surface in negligible amounts. The surface of the organic waste-derived microparticles contains 11.49% oxygen and 87.84% carbon. The high-resolution curve-fitting XPS spectrum of C 1s (Fig. 3e) reveals peaks at 284.12, 284.8, 286.76, and 288.42 eV, corresponding to C=C bonds in aromatic rings,[56] C–C bonds,[64] C–O bonds[64,65] from the primary components of SCG (cellulose, hemicellulose, and lignin), and C=O and O=C–O bonds,[66–68] respectively. The C=O groups are attributed to hemicellulose, while the carboxylic acid group is associated with fatty acids in SCG. Linoleic acid (36.8%), palmitic acid (32.8%), and oleic acid (11.1%) are identified as the predominant fatty acids in SCG.[69] The presence of these saturated and unsaturated fatty acids, bearing a carboxyl group and an aliphatic chain, can lower the surface energy of the interface.[70,71] The O 1s XPS spectrum of RSCG was closely examined to monitor the carboxylic acid (Fig. 3f). The O=C–O stretching of the carboxyl group was detected at a binding energy of 535.1 eV,[56] constituting 16.15% of the spectrum. Multiplying this percentage by the O content (yielding a value of 1.85%) provides a measure to determine the presence of oily content on the surface of the RSCG interface. Additionally, a deconvoluted peak at 532.55 eV,[44,72] representing 83.85% of the spectrum, corresponds to the ether and alcohol functional groups of SCG's cellulose, hemicellulose, and lignin.

To further understand the changes induced by the annealing process, the XPS analysis of HSCG was performed, with the survey spectrum presented in Fig. 3g. A comparison of the C/O ratio between RSCG and HSCG reveals a slight decrease from 7.64 to 6.55 after annealing. This shift in elemental composition is further elucidated by the high-resolution XPS spectrum of C 1s for HSCG (Fig. 3h), which shows a notable increase in the percentage of C–C bonds, rising to 76.65%, a significant 10% increase compared to RSCG. Additionally, the spectrum also shows an increase in the C=O and O=C–O bond content. These observations point to an increase in hydrocarbon chains and carboxylic acid groups on the surface, suggesting an enhanced presence of fatty acids on the HSCG compared to the RSCG. This inference is further corroborated by the analysis of the O 1s XPS spectrum (Fig. 3i), where the proportion of O=C–O functional groups in HSCG reaches 26.55%. When this percentage is multiplied by the total oxygen content of the HSCG, the resulting value of 3.49% indicates an 88% increase in oily substances on the surface of the annealed sample compared to RSCG.

This substantial increase in surface fatty acids following the annealing process aligns with previous studies demonstrating the migration of oily or waxy substances, such as fatty acids, to the surface during thermal treatments. Fatty acids are well-recognized as natural hydrophobic compounds and have been widely utilized in fabricating superhydrophobic coatings.[9] Their presence at the surface induces a low-energy interface, contributing to the lotus effect, a characteristic feature of superhydrophobic surfaces.[73] These natural waxes[74] are known for their limited solubility in many solvents and particularly low solubility in alcohols.[9] Furthermore, they tend to migrate to the surface, improving interface hydrophobicity. For instance, Zhu *et al.* observed a significant increase in the hydrophobicity of a cellulose-based film upon annealing, attributed to the migration of natural waxes from the interior to the film's surface.[75] It is important to note that the annealing temperature used in our study (90 °C) was higher than the melting point of the major fatty acid constituents of SCG; for example, palmitic acid has a reported melting point of 62.8-63 °C.[76] This relatively low melting point increases the mobility of fatty acids during the annealing process, promoting their migration to the surface. Additionally, as the absorbed moisture on the RSCG surface evaporates during annealing (as confirmed by FTIR and TGA data), it is replaced by air molecules. Given that the SCG microparticles were processed via electrospraying, the resultant micro-structured interface exhibits high surface roughness, which enhances air entrapment between the microparticles, forming an air cushion.[53,77]

The micro-structured HSCG interface, with a low surface energy imparted by the modulation of fatty acids, conforms to the Cassie-Baxter wetting model,[78] and exhibits superhydrophobicity (Fig. 3j). Surfaces in the Cassie-Baxter state typically exhibit a low water rolling-off angle and minimal adhesion force, enabling water droplets to easily roll off.

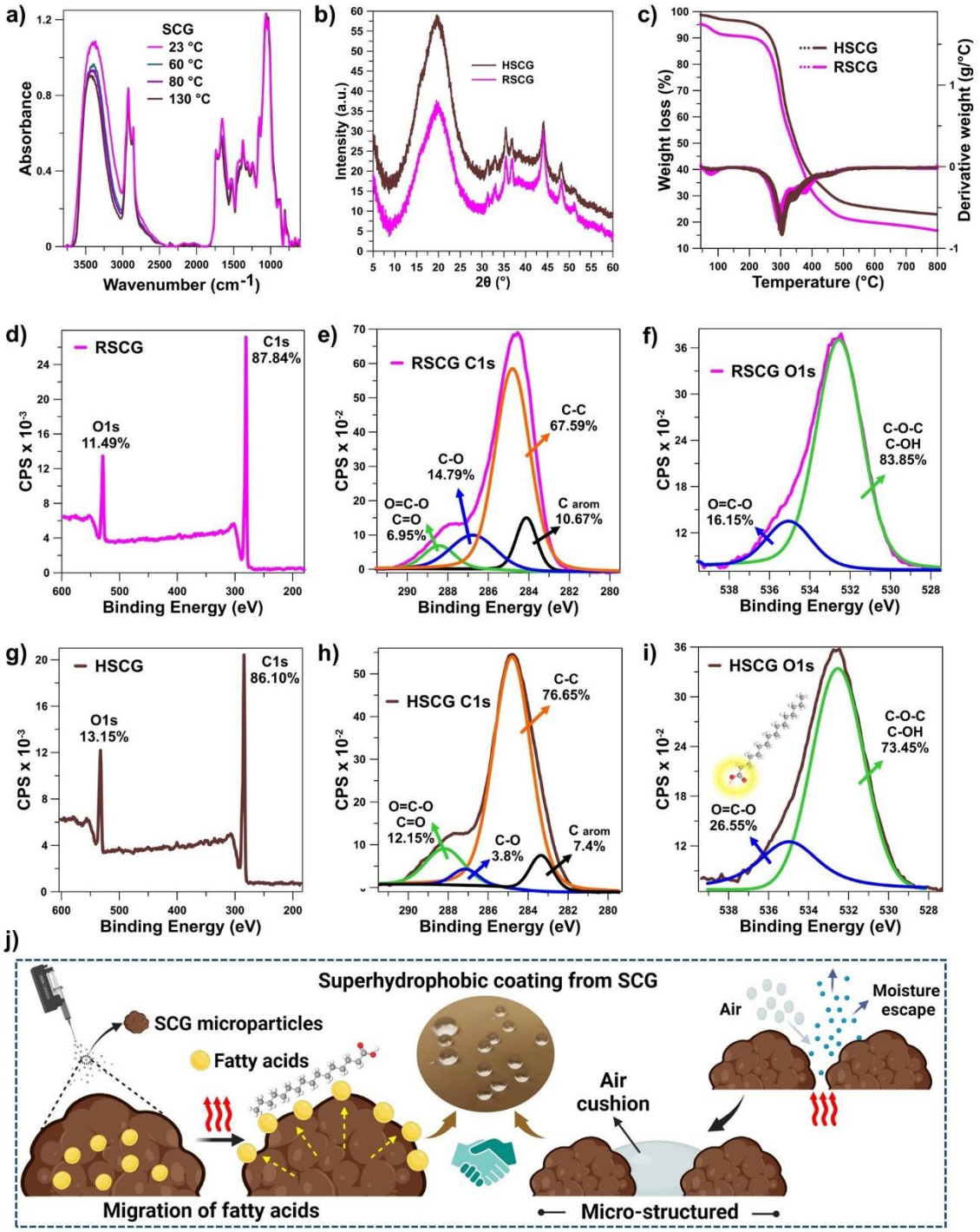

Figure 3: Analysis of RSCG and HSCG interfaces: the impact of annealing on the chemical and physical properties. a) FTIR spectra of RSCG under a temperature ramp. b) XRD patterns of RSCG and HSCG indicate preserved structural integrity post-annealing. c) TGA and DTGA profiles comparing the thermal behavior of RSCG and HSCG. d-i) XPS spectra, including survey and high-resolution C 1s and O 1s spectra, showing surface composition changes after annealing. j) Schematic illustration of the formation of a superhydrophobic surface from SCG in HSCG, depicting the cooperation of surface chemistry and microstructure through fatty acid migration and air cushion formation.

In the subsequent step, the UV-Vis-NIR spectra of both HSCG and RSCG were measured to assess their optical properties (Fig. 4a and b). Both interfaces exhibited similar spectral patterns across the measured wavelength range. However, HSCG demonstrated significantly higher absorbance in the UV region, particularly in the UV-C and UV-B ranges, compared to RSCG (Fig. 4a). As the wavelength transitioned into the visible and NIR regions, the absorbance levels of both samples became nearly identical. The increased UV absorbance in HSCG can be attributed to the higher concentration of fatty acids on its surface, as confirmed by the XPS analysis. Unsaturated fatty acids are known to absorb UV radiation due to double bonds (π-π^* transitions),[79] dissipating the absorbed energy through non-radiative processes such as vibrational relaxation. For example, coconut and olive oil, rich in unsaturated fatty acids such as oleic and linoleic acids, have been shown to absorb UV rays in the UV-B region.[80,81] It should be noted that SCG is also abundant in such fatty acids. The absorption in the UV-B region, as seen in HSCG, suggests potential activity as a natural sunscreen, further highlighting the role these fatty acids play on the surface in light absorption. Furthermore, the reflectance spectra of HSCG and RSCG (Fig. 4b) were identical in the UV region, indicating similar reflective properties. However, a significant difference was observed in the NIR region, where RSCG displayed higher reflectance values than HSCG. This divergence in reflectance could also be linked to the surface composition and structure differences between the two samples.

Following the analysis of UV-Vis-NIR properties, we examined the photothermal capabilities of SCG, particularly its ability to absorb sunlight and convert it into heat (Fig. 4c). The photothermal properties of SCG arise from the presence of melanoidins.[82,83] Melanoidins, products of the Maillard reaction during the roasting of coffee beans, are distinguished by their characteristic brown color and a broad absorption spectrum spanning from UV to NIR wavelengths.[84] Aromatic rings within the melanoidin structure enable the transition of electrons to an excited π^* state upon light absorption.[85] As these excited electrons return to their ground state, a significant portion of the absorbed energy is released as heat through non-radiative relaxation mechanisms. The ability of melanoidins to efficiently convert absorbed light into heat positions them as promising materials for light-to-heat energy conversion applications. Indeed, we observed a remarkably rapid temperature increase on the RSCG interface under solar light irradiation (Fig. 4d). The temperature rose to 60 °C within just 4 s of exposure and reached 70 °C after 10 s. These results confirm that RSCG, an interface composed of SCG microparticles with a thickness of 60 μm, exhibits a robust photothermal response, effectively converting absorbed sunlight into heat (Fig. 4e). It should be noted that during the assessment of the interface's photothermal performance, the platform was placed in an open-air setting to simulate outdoor conditions, where the interface would be exposed to direct sunlight without surrounding barriers. Such an environment is more representative of real-world applications like solar energy harvesting, outdoor thermal management, or protective coatings, where efficient sunlight-to-heat conversion under atmospheric conditions is critical. The temporal temperature profile of the RSCG interface on aluminum foil under one sun irradiation is illustrated in Fig. 4f. Notably, the finely micro-structured interface achieved a temperature increase to 70 °C, eventually stabilizing at 72 °C during the 10-min test, resulting in a temperature difference (ΔT) of 48°C after continuous irradiation. Fig. 4g illustrates the photothermal cycling behavior of RSCG under an on-off solar irradiation protocol (one sun, 1000 W/m^2) over eight cycles. The ΔT of 48 °C remained nearly constant throughout the repeated cycles, demonstrating the photostability of the micro-structured SCG, which is advantageous for long-term practical applications.

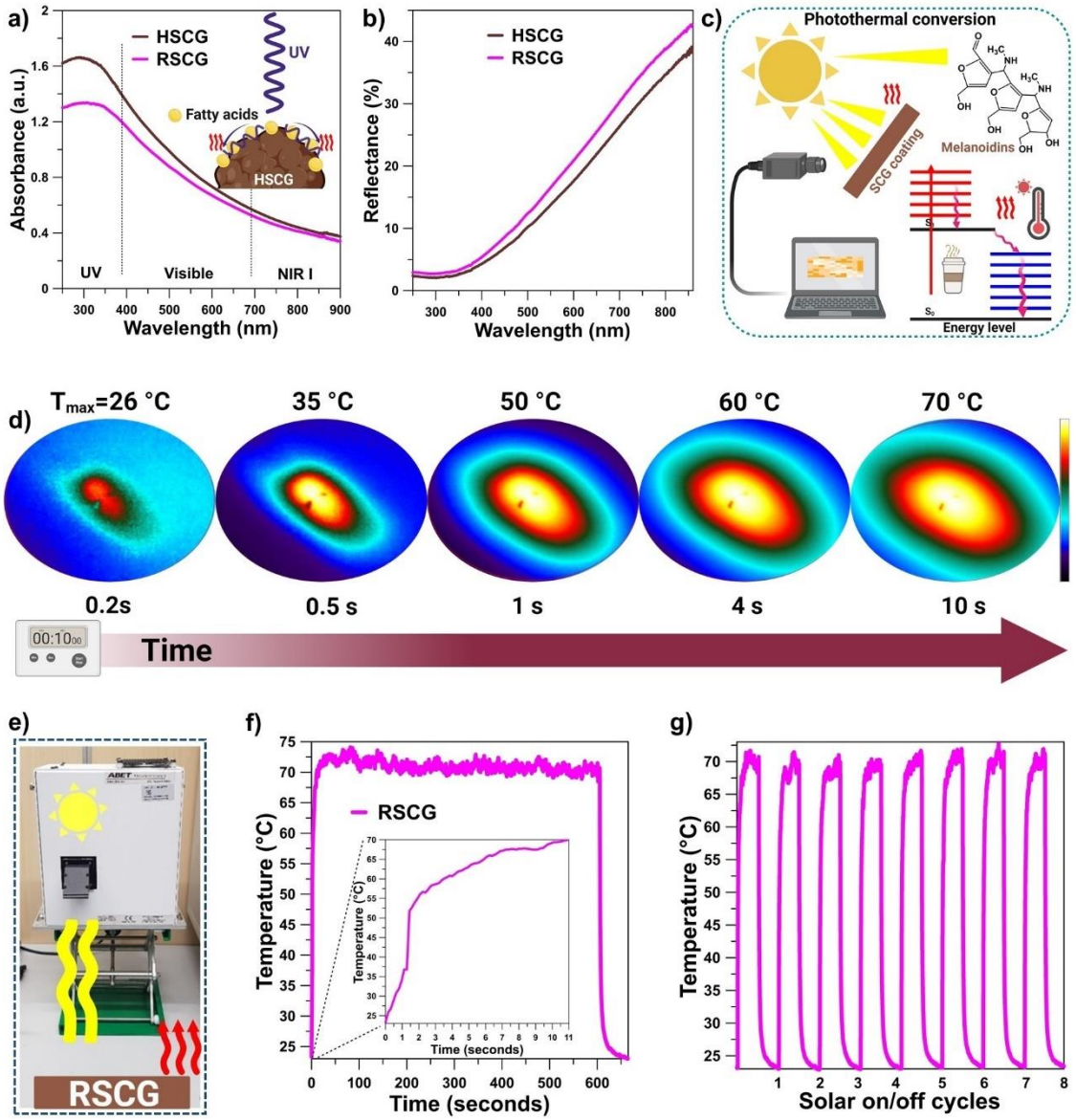

Figure 4. Optical and photothermal properties of RSCG and HSCG interfaces. UV-Vis-NIR a) absorbance and b) reflectance spectra of RSCG and HSCG, showing higher UV absorption in HSCG due to the increased concentration of surface fatty acids. c) Schematic representation of the photothermal conversion mechanism in SCG, driven by the presence of melanoidins. Structural representation of melanoidins is adapted from the work of Bruhns *et al*.[86] d) Thermal camera recordings demonstrating the rapid temperature increase of the RSCG interface under solar irradiation. e) Solar simulator setup. f) Temporal temperature profile of the RSCG under continuous one-sun irradiation. (f) Photothermal cycling behavior of RSCG under on-off solar irradiation.

We further investigated whether the solar-induced heating of the micro-structured SCG interface could serve as an alternative to the annealing process in inducing superhydrophobicity. Given that the annealing process led to the migration of lipids to the surface of the SCG, a key mechanism underlying the observed superhydrophobicity, it was hypothesized that prolonged solar irradiation

might replicate this effect by similarly driving lipid migration through the heat generated during photothermal conversion.

To explore this, RSCG was subjected to extended solar irradiation using a solar simulator, with systematic measurements of contact angle and rolling-off angle taken at 1 h intervals over 6 h (Fig. 5a). Remarkably, after 4 h of continuous irradiation, the RSCG exhibited a significant increase in hydrophobicity, achieving a contact angle of 138°. The observation suggests that the heat generated during irradiation was sufficient to induce the modulation of fatty acids, much like the annealing process. By the end of the 6-hour irradiation period, the interface reached a level of superhydrophobicity comparable to that obtained through annealing (HSCG), with a contact angle of 151° and a rolling-off angle of 9°. These findings demonstrate the effectiveness of solar-induced photothermal heating in modifying the surface properties of SCG microparticles due to their inherent photothermal properties. A potential application is proposed in Fig. 5b. A conceptual model of a house with a roof electrosprayed by SCG is depicted, where prolonged exposure to sunlight naturally induces a superhydrophobic surface. Such an interface could enhance the self-cleaning properties of building materials, reducing maintenance costs and extending the lifespan of structures. Moreover, the ease of SCG electrospraying onto various surfaces, including paper (Sup. Fig. 6), demonstrates the broad applicability of this approach.

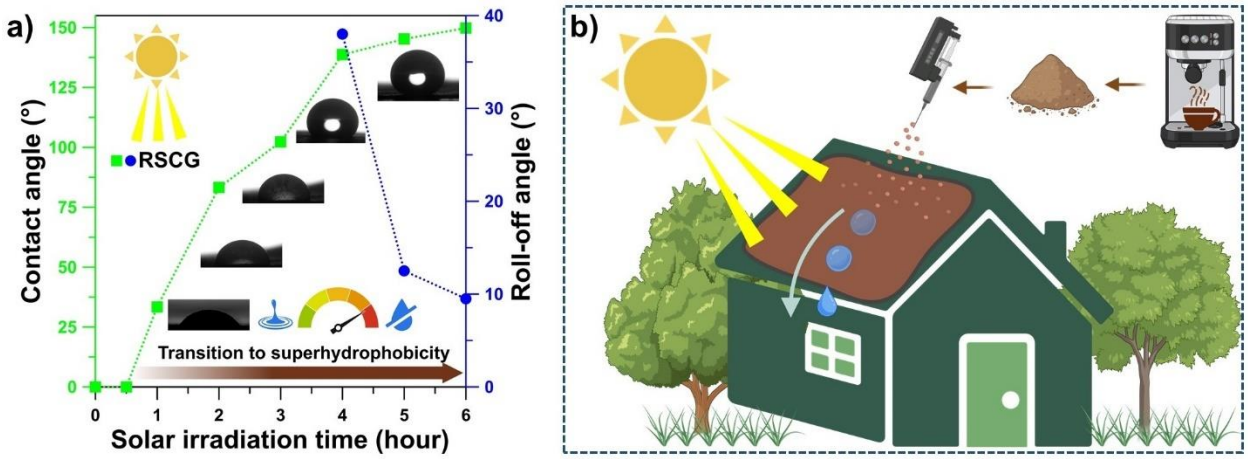

Figure 5: Solar-induced superhydrophobicity of micro-structured SCG interface. a) Evolution of contact angle and rolling-off angle of RSCG under extended solar irradiation, showing the development of superhydrophobicity after 6 hours of irradiation b) Conceptual illustration of a roof coated with SCG microparticles, where prolonged sunlight exposure naturally induces a superhydrophobic surface.

4 Conclusion

This study successfully demonstrated the potential of using SCG as a sustainable material for developing superhydrophobic interfaces. SCG microparticles were transformed into micro-structured interfaces via the electrospraying method. The key findings indicate that after annealing, the SCG interfaces exhibited a high contact angle and a low rolling-off angle, confirming the surface's superhydrophobic nature. XPS analysis revealed that the migration of fatty acids to the SCG surface during the annealing process played a crucial role in lowering the surface energy, contributing to the observed superhydrophobicity. The modulation of surface composition highlights the inherent ability of biowaste materials to achieve special wettability through minimal

processing. Notably, the study also explored the potential for solar-induced heating as an alternative to annealing. Prolonged solar irradiation (up to 6 h) led to similar superhydrophobic characteristics, with the contact angle reaching 151° and the rolling-off angle at 9°. Our experiments demonstrated that sunlight alone can induce the migration of SCG's surface-active compounds, thus eliminating the need for energy-intensive thermal treatments. The implications of these results are profound, particularly in the context of sustainability and practical applications, and align with the United Nations' Sustainable Development Goals[87] by reducing the need for external energy inputs and minimizing the environmental impact of material processing. Our approach's sustainability is reinforced by using SCG, an abundant and renewable waste material, as the primary component of the interface. Moreover, achieving superhydrophobicity through mere exposure to sunlight leverages naturally abundant solar energy to effectuate surface modifications, offering a low-cost, environmentally friendly alternative to conventional thermal treatment methods. Repurposing SCG in this innovative manner contributes to the circular economy, reducing waste while producing value-added products with enhanced functionality.

Author contributions

Seyed Shahrooz Zargarian: conceptualization, validation, resources, investigation, methodology, writing – original draft, writing – review & editing, supervision, project administration, funding acquisition. Javier Saiz-Poseu and Salvio Suárez-García: investigation (XPS, FTIR, SEM, and contact angle measurements), methodology, writing – original draft, writing – review & editing. Daniel Ruiz-Molina: review & editing, supervision. Filippo Pierini: review & editing, supervision, project administration, funding acquisition.

Declaration of competing interest

The authors declare no conflict of interest.

Data availability

Data will be made available on request.

Acknowledgments

This project was supported by HORIZON TMA MSCA Postdoctoral Fellowships - European Fellowships (HORIZON-TMA-MSCA-PF-EF) action program under the call MSCA Postdoctoral Fellowships 2021 (HORIZON-MSCA-2021-PF-01) to S.S.Z., grant agreement No. 101068036, "SuSCoFilter". The authors thank Magdalena Osial for performing the TGA and UV-Vis-NIR analysis and Kamil Bochenek for executing the ball-milling process. Fig. 1-5 were partially created with BioRender. F.P. acknowledges the financial support from the Polish Ministry of Science and Higher Education through a scholarship for outstanding young scientists. This work was also supported by grant PID2021–127983OB-C21 funded by MICIU/AEI/10.13039/501100011033/ and "ERDF A way of making Europe". The ICN2 is funded by the CERCA program/Generalitat de Catalunya and supported by the Severo Ochoa Centres of Excellence programme, Grant CEX2021-001214-S, funded by MICIU/AEI/10.13039.50110001103.

References

(1) *Liravi, M.; Pakzad, H.; Moosavi, A.; Nouri-Borujerdi, A. A comprehensive review on recent advances in superhydrophobic surfaces and their applications for drag reduction. Progress in Organic Coatings* ***2020****, 140, 105537.*

(2) *Wang, S.; Liu, K.; Yao, X.; Jiang, L. Bioinspired Surfaces with Superwettability: New Insight on Theory, Design, and Applications. Chem. Rev.* ***2015****, 115, 8230–8293.*

(3) *Ashok Kumar, S. S.; Bashir, S.; Ramesh, K.; Ramesh, S. A comprehensive review: Super hydrophobic graphene nanocomposite coatings for underwater and wet applications to enhance corrosion resistance. FlatChem* ***2022****, 31, 100326.*

(4) *Rasouli, S.; Rezaei, N.; Hamedi, H.; Zendehboudi, S.; Duan, X. Superhydrophobic and superoleophilic membranes for oil-water separation application: A comprehensive review. Mater. Des.* ***2021****, 204, 109599.*

(5) *Elzaabalawy, A.; Meguid, S. A. Effect of surface topology on the wettability of superhydrophobic surfaces. J Dispers Sci Technol* ***2019****, 1–9.*

(6) *Cortese, B.; D'Amone, S.; Manca, M.; Viola, I.; Cingolani, R.; Gigli, G. Superhydrophobicity due to the hierarchical scale roughness of PDMS surfaces. Langmuir* ***2008****, 24, 2712–2718.*

(7) *Chakraborty, A.; Mulroney, A. T.; Gupta, M. C. Superhydrophobic surfaces by microtexturing: A critical review. In Progress in adhesion and adhesives; Mittal, K. L., Ed.; Wiley, 2021; pp. 621–649.*

(8) *Kong, T.; Luo, G.; Zhao, Y.; Liu, Z. Bioinspired superwettability micro/nanoarchitectures: fabrications and applications. Adv. Funct. Mater.* ***2019****, 29.*

(9) *Bayer, I. S. Superhydrophobic Coatings from Ecofriendly Materials and Processes: A Review. Adv. Mater. Interfaces* ***2020****, 7, 2000095.*

(10) *Lin, W.; Cao, M.; Olonisakin, K.; Li, R.; Zhang, X.; Yang, W. Superhydrophobic materials with good oil/water separation and self-cleaning property. Cellulose* ***2021****, 28, 10425–10439.*

(11) *Hossain, M. M.; Wu, S.; Nasir, A.; Mohotti, D.; Robinson, N. A.; Yuan, Y.; Agyekum-Oduro, E.; Akter, A.; Bhuiyan, K. A.; Ahmed, R.; et al. Superhydrophobic and superoleophilic surfaces prepared by one-step plasma polymerization for oil-water separation and self-cleaning function. Surfaces and Interfaces* ***2022****, 35, 102462.*

(12) *Ma, W.; Ding, Y.; Zhang, M.; Gao, S.; Li, Y.; Huang, C.; Fu, G. Nature-inspired chemistry toward hierarchical superhydrophobic, antibacterial and biocompatible nanofibrous membranes for effective UV-shielding, self-cleaning and oil-water separation. J. Hazard. Mater.* ***2020****, 384, 121476.*

(13) *Xu, D.; Gong, M.; Li, S.; Zhu, X.; Kong, X. Z. Fabrication of superhydrophobic/oleophilic membranes by chemical modification of cellulose filter paper and their application trial for oil–water separation. Cellulose* ***2020****, 27, 6093–6101.*

(14) *Duan, H.; Lyu, H.; Shen, B.; Tian, J.; Pu, X.; Wang, F.; Wang, X. Superhydrophobic-superoleophilic biochar-based foam for high-efficiency and repeatable oil-water separation. Sci. Total Environ.* ***2021****, 780, 146517.*

(15) *Guo, Y.; Zhou, X.; Yi, X.; Wang, D.; Xu, Q. Superhydrophobic behaviors of nanoSiO2 coating on stainless steel mesh and its application in oil/water separation. Appl. Nanosci.* ***2020****, 10, 1511–1520.*

(16) *Makoś-Chełstowska, P.; Słupek, E.; Małachowska, A. Superhydrophobic sponges based on green deep eutectic solvents for spill oil removal from water. J. Hazard. Mater.* ***2022****, 425, 127972.*

(17) *Yang, H.-R.; Huang, Y.-H.; Wang, C.-F.; Chung, T.-S. Green fabrication of PVDF superhydrophobic membranes using a green solvent triethyl phosphate (TEP) for membrane distillation. Desalination* ***2023****, 566, 116934.*

(18) *Zhou, W.; Yu, X.; Li, Y.; Jiao, W.; Si, Y.; Yu, J.; Ding, B. Green-Solvent-Processed Fibrous Membranes with Water/Oil/Dust-Resistant and Breathable Performances for Protective Textiles. ACS Appl. Mater. Interfaces* ***2021****, 13, 2081–2090.*

(19) *Zhang, Y.; Sam, E. K.; Liu, J.; Lv, X. Biomass-Based/Derived Value-Added Porous Absorbents for Oil/Water Separation. Waste Biomass Valor.* ***2023****, 14, 3147–3168.*

(20) *Li, Z.; Zhong, L.; Zhang, T.; Qiu, F.; Yue, X.; Yang, D. Sustainable, flexible, and superhydrophobic functionalized cellulose aerogel for selective and versatile oil/water separation. ACS Sustain. Chem. Eng.* ***2019****, 7, 9984–9994.*

(21) *Wang, F.; Chang, R.; Ma, R.; Tian, Y. Eco-friendly and superhydrophobic nano-starch based coatings for self-cleaning application and oil-water separation. Carbohydr. Polym.* ***2021****, 271, 118410.*

(22) *Wu, D.; Hu, S.; Lu, B.; Hu, Y.; Wang, M.; Yu, W.; Wang, G.-G.; Zhang, J. Waste to treasure: Superwetting foam enhanced by bamboo powder for sustainable on-demand oil-water separation. J. Hazard. Mater.* ***2023****, 441, 129829.*

(23) *Lee, B. H.; Nam, T. G.; Kim, S. Y.; Chun, O. K.; Kim, D.-O. Estimated daily per capita intakes of phenolics and antioxidants from coffee in the Korean diet. Food Sci Biotechnol* ***2018****, 28, 1–11.*

(24) *Martins, A. M.; Marto, J. M. A sustainable life cycle for cosmetics: From design and development to post-use phase. Sustainable Chemistry and Pharmacy* ***2023****, 35, 101178.*

(25) *Singh, T. A.; Pal, N.; Sharma, P.; Passari, A. K. Spent coffee ground: transformation from environmental burden into valuable bioactive metabolites. Rev Environ Sci Biotechnol* ***2023****, 22, 887–898.*

(26) *Saberian, M.; Li, J.; Donnoli, A.; Bonderenko, E.; Oliva, P.; Gill, B.; Lockrey, S.; Siddique, R. Recycling of spent coffee grounds in construction materials: A review. J. Clean. Prod.* ***2021****, 289, 125837.*

(27) *Karmee, S. K. A spent coffee grounds based biorefinery for the production of biofuels, biopolymers, antioxidants and biocomposites. Waste Manag.* ***2018****, 72, 240–254.*

(28) *Solomakou, N.; Tsafrakidou, P.; Goula, A. M. Valorization of SCG through Extraction of Phenolic Compounds and Synthesis of New Biosorbent. Sustainability* ***2022****, 14, 9358.*

(29) *Mussatto, S. I.; Carneiro, L. M.; Silva, J. P. A.; Roberto, I. C.; Teixeira, J. A. A study on chemical constituents and sugars extraction from spent coffee grounds. Carbohydr. Polym.* ***2011****, 83, 368–374.*

(30) *Kovalcik, A.; Obruca, S.; Marova, I. Valorization of spent coffee grounds: A review. Food and Bioproducts Processing* ***2018****, 110, 104–119.*

(31) *Janissen, B.; Huynh, T. Chemical composition and value-adding applications of coffee industry by-products: A review. Resources, Conservation and Recycling* ***2018****, 128, 110–117.*

(32) *Yang, L.; He, Q. S.; Havard, P.; Corscadden, K.; Xu, C. C.; Wang, X. Co-liquefaction of spent coffee grounds and lignocellulosic feedstocks. Bioresour. Technol.* ***2017****, 237, 108–121.*

(33) *Cuccarese, M.; Brutti, S.; De Bonis, A.; Teghil, R.; Di Capua, F.; Mancini, I. M.; Masi, S.; Caniani, D. Sustainable Adsorbent Material Prepared by Soft Alkaline Activation of Spent Coffee Grounds: Characterisation and Adsorption Mechanism of Methylene Blue from Aqueous Solutions. Sustainability* ***2023****, 15, 2454.*

(34) *Shi, C.; Chen, Y.; Yu, Z.; Li, S.; Chan, H.; Sun, S.; Chen, G.; He, M.; Tian, J. Sustainable and superhydrophobic spent coffee ground-derived holocellulose nanofibers foam for continuous oil/water separation. Sustainable Materials and Technologies* ***2021****, 28, e00277.*

(35) *Darmanin, T.; Guittard, F. Recent advances in the potential applications of bioinspired superhydrophobic materials. J. Mater. Chem. A* ***2014****, 2, 16319–16359.*

(36) *Liu, S.; Gao, Y.; Ma, Y.; Meng, T.; Yi, C.; Xu, Z.; Peng, B.; Deng, Z. Ultrasonication-Assisted Waterborne Synthesis of Self-Restorable Superhydrophobic Surfaces with Prolonged Lifespan in Oil Collection. Adv. Mater. Interfaces* ***2021****, 8.*

(37) *Vatanpour, V.; Kose-Mutlu, B.; Koyuncu, I. Electrospraying technique in fabrication of separation membranes: A review. Desalination* ***2022****, 533, 115765.*

(38) *Jaworek, A. Micro- and nanoparticle production by electrospraying. Powder Technol.* ***2007****, 176, 18–35.*

(39) *Yoon, H.; Kim, H.; Latthe, S. S.; Kim, M.; Al-Deyab, S.; Yoon, S. S. A highly transparent self-cleaning superhydrophobic surface by organosilane-coated alumina particles deposited via electrospraying. J. Mater. Chem. A* ***2015****, 3, 11403–11410.*

(40) *Park, J. Y.; Oh, K. O.; Won, J. C.; Han, H.; Jung, H. M.; Kim, Y. S. Facile fabrication of superhydrophobic coatings with polyimide particles using a reactive electrospraying process. J Mater Chem* ***2012****, 22, 16005.*

(41) *Conde, J. J.; Ferreira-Aparicio, P.; Chaparro, A. M. Anti-corrosion coating for metal surfaces based on superhydrophobic electrosprayed carbon layers. Applied Materials Today* ***2018****, 13, 100–106.*

(42) *Zargarian, S. S.; Kupikowska-Stobba, B.; Kosik-Kozioł, A.; Bartolewska, M.; Zakrzewska, A.; Rybak, D.; Bochenek, K.; Osial, M.; Pierini, F. Light-responsive biowaste-derived and bio-inspired textiles: Dancing between bio-friendliness and antibacterial functionality. Materials Today Chemistry* ***2024****, 41, 102281.*

(43) *Atabani, A. E.; Al-Rubaye, O. K. Valorization of spent coffee grounds for biodiesel production: blending with higher alcohols, FT-IR, TGA, DSC, and NMR characterizations. Biomass Conv. Bioref.* ***2022****, 12, 577–596.*

(44) *Mukherjee, A.; Borugadda, V. B.; Dynes, J. J.; Niu, C.; Dalai, A. K. Carbon dioxide capture from flue gas in biochar produced from spent coffee grounds: Effect of surface chemistry and porous structure. Journal of Environmental Chemical Engineering* ***2021****, 9, 106049.*

(45) *Bejenari, V.; Marcu, A.; Ipate, A.-M.; Rusu, D.; Tudorachi, N.; Anghel, I.; Şofran, I.-E.; Lisa, G. Physicochemical characterization and energy recovery of spent coffee grounds. Journal of Materials Research and Technology* ***2021****, 15, 4437–4451.*

(46) *Tala, W.; Chantara, S. Use of spent coffee ground biochar as ambient PAHs sorbent and novel extraction method for GC-MS analysis. Environ. Sci. Pollut. Res. Int.* ***2019****, 26, 13025–13040.*

(47) *He, T.; Jokerst, J. V. Structured micro/nano materials synthesized via electrospray: a review. Biomater Sci* ***2020****, 8, 5555–5573.*

(48) *Gan, Y.; Zhang, X.; Li, H.; Tong, Y.; Shi, Y.; Yan, Y. The atomization current and droplet size of ethanol in two different small-scale electro-spraying systems. J. Electrostat.* ***2017****, 87, 228–235.*

(49) *Dufour, R.; Perry, G.; Harnois, M.; Coffinier, Y.; Thomy, V.; Senez, V.; Boukherroub, R. From micro to nano reentrant structures: hysteresis on superomniphobic surfaces. Colloid Polym Sci* ***2013****, 291, 409–415.*

(50) *Modesto-Lopez, L. B.; Biswas, P. Role of the effective electrical conductivity of nanosuspensions in the generation of TiO2 agglomerates with electrospray. J. Aerosol Sci.* ***2010****, 41, 790–804.*

(51) *Liu, C.; Bonaccurso, E.; Butt, H.-J. Evaporation of sessile water/ethanol drops in a controlled environment. Phys. Chem. Chem. Phys.* ***2008****, 10, 7150–7157.*

(52) *Xu, T.; Rodriguez-Martinez, V.; Sahasrabudhe, S. N.; Farkas, B. E.; Dungan, S. R. Effects of temperature, time and composition on food oil surface tension. Food Biophys* ***2017****, 12, 88–96.*

(53) *Zha, Q.; Chen, X.; Wang, G.; Chen, Y.; Yang, C.; Yin, Z.; Liu, K.; Luo, Y.; Hong, Z.; Xue, M. A simple strategy towards construction of copper foam-based robust superhydrophobic coating based on perpendicular nanopins for long-lasting delayed icing and reduced frosting. Colloids and Surfaces A: Physicochemical and Engineering Aspects* ***2024****, 690, 133798.*

(54) *Soares, B.; Gama, N.; Freire, C. S. R.; Barros-Timmons, A.; Brandão, I.; Silva, R.; Neto, C. P.; Ferreira, A. Spent coffee grounds as a renewable source for ecopolyols production. J. Chem. Technol. Biotechnol.* ***2015****, 90, 1480–1488.*

(55) *Ballesteros, L. F.; Teixeira, J. A.; Mussatto, S. I. Chemical, functional, and structural properties of spent coffee grounds and coffee silverskin. Food Bioprocess Technol.* ***2014****, 7, 3493–3503.*

(56) *Shin, J.; Kwak, J.; Lee, Y.-G.; Kim, S.; Son, C.; Cho, K. H.; Lee, S.-H.; Park, Y.; Ren, X.; Chon, K. Changes in adsorption mechanisms of radioactive barium, cobalt, and strontium ions using spent coffee waste biochars via alkaline chemical activation: Enrichment effects of O-containing functional groups. Environ. Res.* ***2021****, 199, 111346.*

(57) *Sermyagina, E.; Mendoza Martinez, C. L.; Nikku, M.; Vakkilainen, E. Spent coffee grounds and tea leaf residues: Characterization, evaluation of thermal reactivity and recovery of high-value compounds. Biomass and Bioenergy* ***2021****, 150, 106141.*

(58) *Caporaso, N.; Whitworth, M. B.; Fisk, I. D. Prediction of coffee aroma from single roasted coffee beans by hyperspectral imaging. Food Chem.* ***2022****, 371, 131159.*

(59) *Andrade, T. S.; Vakros, J.; Mantzavinos, D.; Lianos, P. Biochar obtained by carbonization of spent coffee grounds and its application in the construction of an energy storage device. Chemical Engineering Journal Advances* ***2020****, 4, 100061.*

(60) *Wei, Y.; Zhou, M.; Yao, A.; Zhu, P. Preparation of Microfibrillated Cellulose from Wood Pulp through Carbamate Modification and Colloid Milling. Appl. Sci.* ***2020****, 10, 1977.*

(61) *Dericiler, K.; Kocanali, A.; Buldu-Akturk, M.; Erdem, E.; Saner Okan, B. Upcycling process of transforming waste coffee into spherical graphene by flash pyrolysis for sustainable supercapacitor manufacturing with virgin graphene electrodes and its comparative life cycle assessment. Biomass Conv. Bioref.* ***2022****.*

(62) *Rufford, T. E.; Hulicova-Jurcakova, D.; Zhu, Z.; Lu, G. Q. A comparative study of chemical treatment by $FeCl_3$, $MgCl_2$, and $ZnCl_2$ on microstructure, surface chemistry, and double-layercapacitance of carbons from waste biomass. J Mater Res* ***2010****, 25, 1451–1459.*

(63) *Owais, A.; Khaled, M.; Yilbas, B. S. 3.9 hydrophobicity and surface finish. In Comprehensive Materials Finishing; Elsevier, 2017; pp. 137–148.*

(64) *Zhu, Y.; Zhang, K.; Hu, Q.; Liu, W.; Qiao, Y.; Cai, D.; Zhu, P.; Wang, D.; Xu, H.; Shu, S.; et al. Accelerated spent coffee grounds humification by heat/base co-activated persulfate and products' fertilization evaluation. Environmental Technology & Innovation* ***2023****, 32, 103393.*

(65) *Chan, H.; Shi, C.; Wu, Z.; Sun, S.; Zhang, S.; Yu, Z.; He, M.; Chen, G.; Wan, X.; Tian, J. Superhydrophilic three-dimensional porous spent coffee ground reduced palladium nanoparticles for efficient catalytic reduction. J. Colloid Interface Sci.* ***2022****, 608, 1414–1421.*

(66) *Ge, X.; Zhang, C.; Meng, M.; Song, Y.; Hu, S.; Gu, Y. Nickel and Molybdenum Composites Decorated Nitrogen-Doped Carbon Catalysts from Spent Coffee Grounds for Alkaline Hydrogen Evolution. Chempluschem* ***2024****, e202300786.*

(67) *Dai, Z.; Ren, P.-G.; Zhang, H.; Gao, X.; Jin, Y.-L. Nitrogen-doped and hierarchically porous carbon derived from spent coffee ground for efficient adsorption of organic dyes. Carbon letters* ***2021****, 31, 1249–1260.*

(68) *Jin, Y.; Tang, W.; Wang, J.; Chen, Z.; Ren, F.; Sun, Z.; Wang, F.; Ren, P. High photocatalytic activity of spent coffee grounds derived activated carbon-supported Ag/TiO2 catalyst for degradation of organic dyes and antibiotics. Colloids and Surfaces A: Physicochemical and Engineering Aspects* ***2022****, 655, 130316.*

(69) *Mota, D. A.; Santos, J. C. B.; Faria, D.; Lima, Á. S.; Krause, L. C.; Soares, C. M. F.; Ferreira-Dias, S. Synthesis of Dietetic Structured Lipids from Spent Coffee Grounds Crude Oil Catalyzed by Commercial Immobilized Lipases and Immobilized Rhizopus oryzae Lipase on Biochar and Hybrid Support. Processes* ***2020****, 8, 1542.*

(70) *Aras, O.; Baydir, E.; Akman, B. Highly durable spray-coated superhydrophobic surface: Pre-anodizing and fatty acid chain length effect. Korean J. Chem. Eng.* ***2022****, 39, 775–784.*

(71) *Zdziennicka, A.; Szymczyk, K.; Jańczuk, B.; Longwic, R.; Sander, P. Surface, Volumetric, and Wetting Properties of Oleic, Linoleic, and Linolenic Acids with Regards to Application of Canola Oil in Diesel Engines. Appl. Sci.* ***2019****, 9, 3445.*

(72) *Yang, S.; Wang, C.; Li, B.; Chen, H.; Wang, J. Removal of Pb2+ from aqueous solution using an MgO nano-hybridized magnetic biochar from spent coffee grounds. Chem. Phys. Lett.* ***2023****, 833, 140894.*

(73) *Saji, V. S. Wax-based artificial superhydrophobic surfaces and coatings. Colloids and Surfaces A: Physicochemical and Engineering Aspects* ***2020****, 602, 125132.*

(74) *Rodríguez-Fabià, S.; Torstensen, J.; Johansson, L.; Syverud, K. Hydrophobisation of lignocellulosic materials part I: physical modification. Cellulose* ***2022****, 29, 5375–5393.*

(75) *Zhu, M.; Ying, D.; Zhang, H.; Xu, X.; Chang, C. Self-healable hydrophobic films fabricated by incorporating natural wax into cellulose matrix. Chemical Engineering Journal* ***2022****, 446, 136791.*

(76) *Ward, T. L.; Singleton, W. S. Physical properties of fatty acids. II. some dilatometric and thermal properties of palmitic acid. J. Phys. Chem.* ***1952****, 56, 696–698.*

(77) *Zhang, J.; Zhang, L.; Gong, X. Large-Scale Spraying Fabrication of Robust Fluorine-Free Superhydrophobic Coatings Based on Dual-Sized Silica Particles for Effective Antipollution and Strong Buoyancy. Langmuir* ***2021****, 37, 6042–6051.*

(78) *Ning, H.; Zhang, T.; Zhang, L.-Z. Application of self-assembly methods in the preparation of superhydrophobic surfaces: A review. Surfaces and Interfaces* ***2024****, 51, 104765.*

(79) *Anil Kumar, K.; Viswanathan, K. Study of UV Transmission through a Few Edible Oils and Chicken Oil. Journal of Spectroscopy* ***2013****, 2013, 1–5.*

(80) *Kaur, C. D.; Saraf, S. In vitro sun protection factor determination of herbal oils used in cosmetics. Pharmacognosy Res.* ***2010****, 2, 22–25.*

(81) *Chu, C. C.; Nyam, K. L. Application of seed oils and its bioactive compounds in sunscreen formulations. J Am Oil Chem Soc* ***2021****, 98, 713–726.*

(82) *Moya-Ramírez, I.; Pegalajar-Robles, M. E.; Debiasi Alberton, M.; Rufián-Henares, J. A.; Fernández-Arteaga, A.; Garcia-Roman, M.; Altmajer-Vaz, D. Spent coffee grounds as feedstock for the production of biosurfactants and the improved recovery of melanoidins. World J Microbiol Biotechnol* ***2023****, 39, 254.*

(83) *Chien, H.-W.; Chen, X.-E. Spent coffee grounds as potential green photothermal materials for biofilm elimination. Journal of Environmental Chemical Engineering* ***2022****, 10, 107131.*

(84) *Lee, M.-Y.; Lee, C.; Jung, H. S.; Jeon, M.; Kim, K. S.; Yun, S. H.; Kim, C.; Hahn, S. K. Biodegradable photonic melanoidin for theranostic applications. ACS Nano* ***2016****, 10, 822–831.*

(85) *Hsieh, P.-C.; Chen, Y.-C.; Zheng, N.-C.; Mangindaan, D.; Chien, H.-W. A low-cost and environmentally-friendly chitosan/spent coffee grounds composite with high photothermal properties for interfacial water evaporation. Journal of Industrial and Engineering Chemistry* ***2023****, 126, 283–291.*

(86) *Bruhns, P.; Kanzler, C.; Degenhardt, A. G.; Koch, T. J.; Kroh, L. W. Basic Structure of Melanoidins Formed in the Maillard Reaction of 3-Deoxyglucosone and γ-Aminobutyric Acid. J. Agric. Food Chem.* ***2019****, 67, 5197–5203.*

(87) THE 17 GOALS | Sustainable Development https://sdgs.un.org/goals (accessed Sep 1, 2024).